Isı Bilimi ve Tekniği Dergisi, 39, 2, 151-161, 2019
J. of Thermal Science and Technology

ISSN 1300-3615

EXPERIMENTAL AND NUMERICAL STUDY ON HEAT TRANSFER PERFORMANCE OF SQUARE, CYLINDRICAL AND PLATE HEAT SINKS IN EXTERNAL TRANSITION FLOW REGIME

Aykut Barış İNCİ* ve Özgür BAYER**
*Department of Mechanical Engineering, Middle East Technical University, Ankara, e162978@metu.edu.tr
**Department of Mechanical Engineering, Middle East Technical University, Ankara, bayer@metu.edu.tr

(Geliş Tarihi: 18.03.2019, Kabul Tarihi: 14.05.2019)

Abstract: Geometrical optimization of heat sinks with square, cylindrical and plate fins for heat transfer increase is numerically analyzed in transition regime external flow. The relations between the thermal characteristics of fins and boundary conditions such as free-stream velocity are investigated. Experimental studies are performed by using manufacturable fins to validate the numerical model. Heat transfer correlations are derived in order to determine average heat transfer coefficients over a certain range of both Reynolds number and non-dimensional geometric parameters like spanwise and streamwise spacings. Confidence level of the experimental work is demonstrated by uncertainty analysis. Cylindrical fins are observed to be approximately 4.5% superior to ones with square and plate profiles in terms of maximum base plate temperature.
Keywords: CFD, external flow, fin, heat sink, transition regime, heat transfer correlation

DIŞ GEÇİŞ AKIŞI REJİMİNDE KARE, SİLİNDİR VE PLAKA ISI KUYULARI İÇİN ISI TRANSFER PERFORMANSI ÜZERİNE DENEYSEL VE SAYISAL ÇALIŞMA

Özet: Kare, silindir ve plaka kanatçıklı ısı kuyularının ısı transferi artışına yönelik geometrik en iyileştirilmeleri geçiş rejimindeki dış akışta sayısal olarak incelenmiştir. Serbest akış hızı gibi sınır koşulları ile kanatçık termal karakterizasyonu arasındaki ilişkiler araştırılmıştır. Sayısal modeli doğrulamak için üretilebilir kanatçıklar kullanılarak deneysel çalışmalar gerçekleştirilmiştir. Ortalama ısı transfer katsayısını belirlemek üzere, hem belirli bir Reynolds sayısı hem de akış yönü ile akışa dik doğrultudaki boyutsuz geometrik parametrelerin aralığı dikkate alınarak ısı transferi korelasyonları elde edilmiştir. Deneysel çalışmanın güvenilirliği belirsizlik analizi ile gösterilmiştir. Taban plakası en yüksek sıcaklığının, silindir kanatçıklı ısı kuyusunda diğerlerine göre yaklaşık %4.5 oranında daha düşük çıktığı gözlemlenmiştir.
Anahtar Kelimeler: HAD, Dış Akış, Kanatçık, Isı Kuyusu, Geçiş Rejimi, Isı Transfer Korelasyonu

NOMENCLATURE

A_{ins}	Heat transfer area of insulation material [m^2]
A_T	Total heat transfer area [m^2]
a,b,c,e	Coefficient of correlations
B	Thickness of base plate [mm]
C.V.	Coefficient of variation
D_h	Characteristic length [mm]
d	Diameter of a cylindrical fin [mm]
e	Specific internal energy [kJ/kg]
H	Height of fin [mm]
h	Specific enthalpy [kJ/kg]
h_{avg}	Average heat transfer coefficient [W/m^2K]
I	Current [A]
k_{air}	Thermal conductivity of air [W/mK]
k_{ins}	Thermal conductivity of insulation [W/mK]
L	Length of base plate [mm]
L_{ins}	Thickness of insulation material [mm]
n	Refinement level
n	Data points
Nu	Nusselt number
Nu_{corr}	Correlated Nusselt number
Nu_{exp}	Experimental Nusselt number
$\overline{Nu_{exp}}$	Mean value of Nu_{exp}
Nu_{num}	Numerical Nusselt number
Q_{conv}	Convection heat transfer rate [W]
Q_{input}	Heat input rate [W]
Q_{ins}	Heat transfer rate through insulation [W]
Q_{rad}	Radiation heat transfer rate [W]
r	Correlation coefficient
r^2	Coefficient of determination
Re	Reynolds number
S_L	Inter-fin spacing in streamwise dir. [mm]
S_T	Inter-fin spacing in spanwise dir. [mm]
S_L/L	Non-dimensional streamwise spacing
S_T/L	Non-dimensional spanwise spacing
S_r	Summation of squares of residuals between data points and correlation points
S_t	Summation of squares of residuals between data points and arithmetic mean
S_y	Standart deviation
$S_{y/x}$	Standart error of estimate
s	Edge length of a square fin [mm]

T_{max}	Maximum temperature on the upper surface of the base plate [℃]
t	Strip thickness of plate fin [mm]
t	Time [s]
t_{ij}	Viscous stress tensor [N/m^2]
u_i, u_j	Velocity in tensor notation [m/s]
U	Free-stream velocity [m/s]
U_{max}	Maximum velocity [m/s]
V	Voltage [V]
y	Predictor variable

Greek Symbols

δ	Deviation of variable
δ_{ij}	Kronecker delta
ΔT	Temperature diff. between top and bottom layers of insulation material [℃]
ΔT_{lm}	Logarithmic mean temperature difference [℃]
η_o	Overall efficiency of fin array
μ	Dynamic viscosity of air [kg/ms]
ν	Kinematic viscosity of air [m^2/s]
ρ	Density of air [kg/m^3]

INTRODUCTION

In the last half century, heat generated by electronic equipment drastically increased and removal of excess heat in more efficient ways became a necessity. In this aspect, Babus'Haq et al. (1995), Diani et al. (2013), Deshmukh (2013), Samarth and Sawankar (2014) numerically and experimentally investigated heat transfer enhancement concepts in fins. Babus'Haq's (1995) experimental work was related to the effect of inter-fin spacing on the thermal performance of a cylindrical pin-fin assembly in a duct under forced convection. Fractions of optimum span-wise and stream-wise spacing values to diameter were found to be 1.04 and 0.95, respectively, for duralumin material, however, the interval of Reynolds number and flow characteristic are not clear. Average convective heat transfer coefficient and pressure drop values with changing frontal velocity for elliptic, square, circular and plate fins in staggered or in-line configurations were investigated by Yang et al. (2007). In this experimental work, constant heat flux is applied to fin configurations in a duct. The results showed that circular pin fins are superior to other fin shapes in terms of average convective heat transfer coefficient for the in-line configuration.

There are different comparison criteria for effectiveness of fins in the literature. Sahiti et al. (2006) numerically compared NACA, dropform, lancet elliptic, circular and square shaped fins located in a duct with respect to two sets of comparison criteria. One set consists of hydraulic diameter, coverage ratio (fin cross section area / bare plate area), and pin length equalities. The other includes blockage area, distance between the pins and pin length equalities. Unlike the results of Yang et al. (2007), elliptical shaped fins had a better performance than others. Jonnson and Moshfegh (2001) experimentally worked on strip, plate circular and square shaped fins by equalizing their frontal area for Reynolds numbers between 2000 and 16500.

Experimental studies on hydrodynamic and thermal characterization of heat sinks were extended to micro scale with nanofluids. Sandhu et al. (2018) recently performed a study with 21 parallel microchannel heat sink and alumina nanofluids with different base fluids. Obtained results show that an increase in the flow rate and nanoparticle concentration promote an increase in heat transfer coefficient. Thermal and hydraulic performances of an air-cooled, planar, oblique-finned heat sink were researched by Kanargi et al (2018). The conjugate heat transfer between the heat sink and the air flow were computed numerically and validated experimentally. Damook et al. (2016) performed a study on the temperature dependency of air properties in numerical simulations for air flows over pinned heat sinks. As expected, numerical simulations taking the temperature-dependent air properties into account are in better agreement with experimental measurements of pressure drop, heat transfer coefficient, and heat sink base temperature.

There are also analytical studies concentrated on optimization of fins with different methods including Yang et al. (2013) and Culham and Muzychka et al. (2001). The study of Chu et al. (2011) investigated the cooling design of a remote radio unit under natural convection. They determined that the optimal fin number is around 25 and the pin-fin heat sink increases the average heat transfer coefficient by 11.2% with a 38.6% decrease in the heat transfer area. Specific to electric vehicle application, Mohammadian et al. (2015) performed a three dimensional transient thermal analysis of an air-cooled module having prismatic Li-ion cells and aluminum pin fin heat sink with increasing fin height in the flow direction. Kwak et al. (2017) performed an experimentally validated numerical work on commercial LED light bulbs considering radial heat sink with triangular fins at different angles. A correlation was obtained for cooling performance for the radial heat sinks with and without triangular fins considering natural convection and radiation.

The present study aims to experimentally and numerically investigate the geometrical optimization of square, cylindrical and plate fins for heat transfer augmentation in the transition regime for external air flow at steady state conditions and specifically targets military applications. Comparison of heat transfer characteristics of optimized geometries is performed. Heat transfer correlations including thermal, hydraulic and geometrical parameters are derived for tested fins with different profiles. Keeping Reynolds number fixed in external flow for different geometry fins specifically in transition regime is the most innovative point in present study.

METHODOLOGY

For valuable and accurate analysis in external transition flow over different fins, geometric and hydraulic parametrization are performed. Experimental and numerical studies are conducted based on parametrization characteristics defining the problem.

Parametrization

Square, cylindrical and plate fins as illustrated in Figure 1 are used in the present study. Fin geometries are selected to be discrete, as sharp edged square and blunt cylinder, and continuous like plate since they are widely used fin geometries in small base area heat sinks. The fins also result in different hydrodynamic characteristics of air flowing over them.

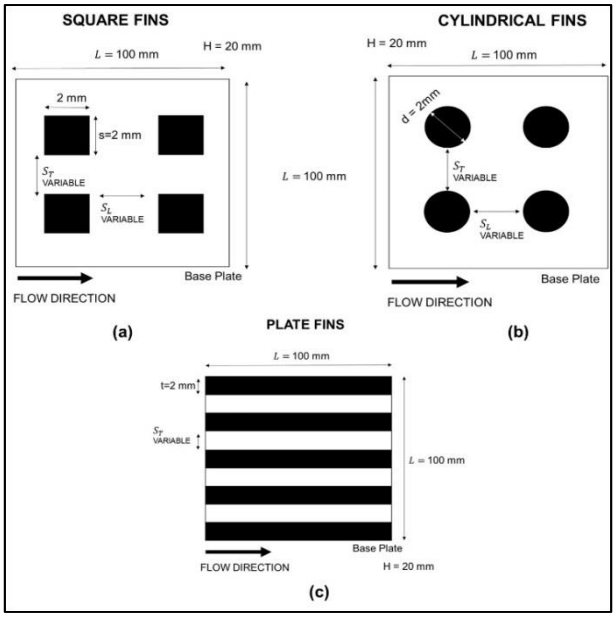

Figure 1. Geometrical properties of (a) square fin, (b) cylindrical fin, (c) plate fin

Dimensions of the base plate (L and B) and height (H) of the fins are kept constant as illustrated in Table 1. Manufacturing concerns limit the ratio between the fin height and inter-fin spacing to a maximum value of 10 for aluminum alloys in milling process which is the most common production technique for a fin array. For known fin geometries, production of fin arrays are more practical if the same volume criterion is selected instead of same surface-to-volume criterion. There are 3 different streamwise (S_L) and spanwise (S_T) spacing values for square and cylindrical fins and 3 different spanwise (S_T) values for plate fins. Each array is characterised by its interfin spacings in free stream area and orthogonal directions as in Tahat et al. (2000).

Table 1. Geometrical parameters of fins

H (mm)	L (mm)	B (mm)	S_L (mm)	S_T (mm)	S_L/L (-)	S_T/L (-)
20	100	10	5.00	5.00	0.0500	0.0500
			3.16	3.16	0.0316	0.0316
			2.08	2.08	0.0208	0.0208

Geometrical optimization is applied for heat transfer augmentation for free stream velocities (U) of 3, 5, and 7 m/s. Heat transfer performances of geometrically optimized fins are compared. The diameter of a cylindrical fin (d), strip thickness of a plate fin (t) and edge length of a square fin (s) are assumed as characteristic length (D_h) and taken as 2 mm. Equalizing thickness or diameter of fins result in the same free-stream area and number of fins in spanwise direction for heat sinks. Free stream area is the area normal to air flow between the fins as shown in Figure 2.

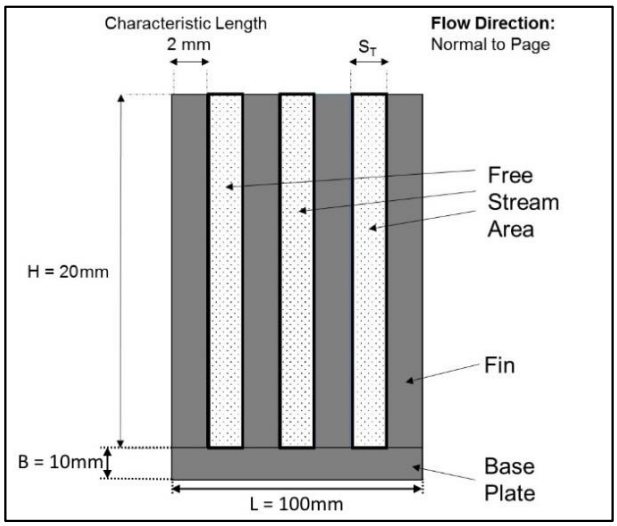

Figure 2. Free stream area in the heat sink

Reynolds number is calculated based on the maximum flow velocity and characteristic length of a single fin as in the studies of Zukauskas (1975) and Khan (2004). Therefore, Reynolds number is kept constant for fins with different profiles and same spanwise spacing.

$$Re = \frac{U_{max} D_h}{\nu} \tag{1}$$

$$U_{max} = U \frac{S_T + 2}{S_T} \tag{2}$$

Reynolds number varies between 528.6 for S_T = 5 mm and U = 3 m/s case, and 750 for S_T = 2 mm and U = 7 m/s case, and the flow is in transition regime according to Zukauskas (1975).

Experimental Study

The experimental setup presented in Figure 3 was constructed in the Heat Transfer Laboratory at Aselsan Gölbaşı Campus. The width, height and length of the tunnel are 600 mm, 400 mm and 1500 mm, respectively.

Pumping power is supplied by two identical axial fans located at the inlet of the tunnel. Flow straighteners are used to get uniform velocity profile. Velocity and temperature profile of the air are measured by 14 hot wire anemometers (7 anemometers for front side, 7 anemometers for back side of the fin). A plate heater that

can operate up to 300 W is produced by casting aluminum over a resistor. The heater has 100 mm × 100 mm cross-section and 10 mm height. A gap pad made of fiberglass-reinforced filler and polymer is placed between the fin and heater to compensate for surface irregularities and decrease the resistance. Stone wool which has 150 mm thickness, 750 mm length and 600 mm width is placed under and near the heater for insulation. J-type thermocouples are used to determine average base plate, bottom surface of the heater and insulation material temperature values. The positions of thermocouples are shown in Figure 4.

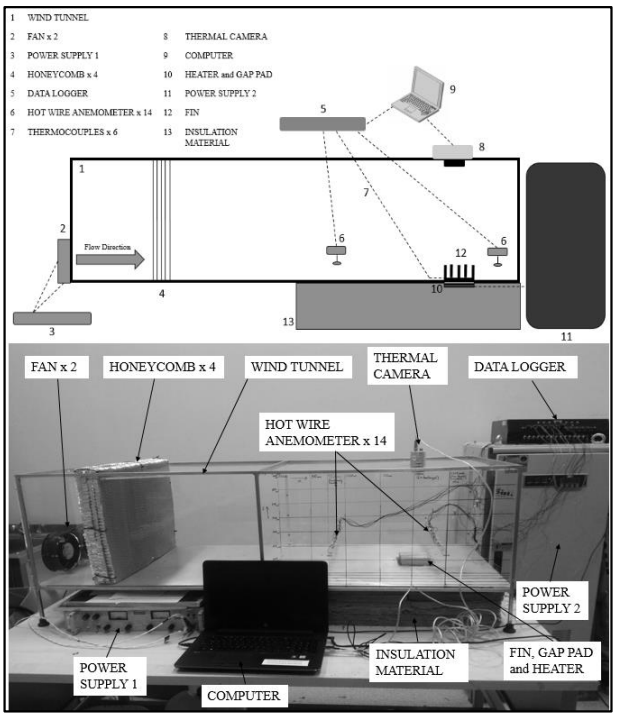

Figure 3. Experimental setup (a) schematic, (b) constructed

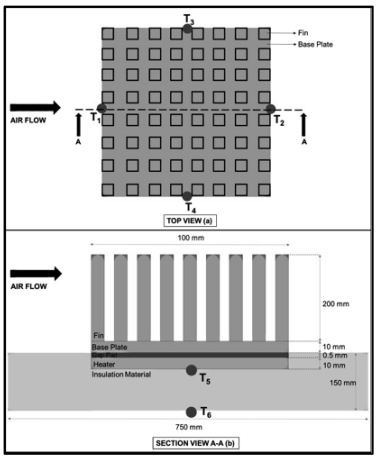

Figure 4. Thermocouples position and location of fin, base plate, gap pad, heater and insulation material from (a) Top view, (b) Section view A-A

Values measured by thermocouples and hot wire anemometers are recorded by a data logger. A thermal camera is used to monitor the temperature distribution on the upper surface of the base plate and to determine the maximum temperature (T_{max}). The thermocouples are calibrated in a thermo bath. Hot wire anemometers, thermal camera and multimeters measuring current and voltage are regularly sent to the suppliers and calibrated according to the standards provided by EURAMET (2018). 15 different fins (6 square, 6 cylindrical, 3 plate) are manufactured from 6063-T6 aluminum alloy. Tape with known emissivity value of 0.95 is stuck to the base plate for more accurate results for thermal camera. Some of the fins can be used by rotating them 90 degrees. Details of geometrical parameters of manufactured fins are presented in Table 2 and Figure 5.

Table 2. Geometrical properties of manufactured fins

Fin Shape	N_L	N_T	S_L (mm)	S_T (mm)	Index
Square	15	15	5.00	5.00	a
		20		3.16	b
		25		2.08	c
	20	15	3.16	5.00	b
		20		3.16	d
		25		2.08	e
	25	15	2.08	5.00	c
		20		3.16	e
		25		2.08	f
Cylindrical	15	15	5.00	5.00	g
		20		3.16	h
		25		2.08	i
	20	15	3.16	5.00	h
		20		3.16	j
		25		2.08	k
	25	15	2.08	5.00	i
		20		3.16	k
		25		2.08	l
Plate	-	15	-	5.00	m
		20		3.16	n
		25		2.08	o

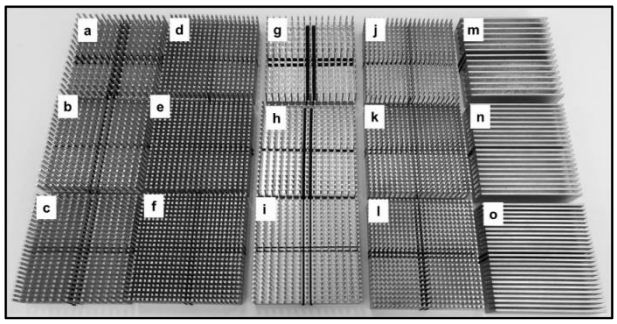

Figure 5. Manufactured fins

Numerical Work

A channel with dimensions of 400 mm (height) × 600 mm (width) × 500 mm (length) is defined in Figure 6. Velocity boundary condition is defined at the inlet of the channel. The fin, gap pad and heater are placed 250 mm away from inlet of the channel. An insulation layer having the same width and length with the channel and 150 mm height is placed below the channel. Numerical domain with dimensions of 750 mm (height) × 800 mm (width) × 750 mm (length) is formed including channel

and insulation for simulating natural convection below the insulation layer.

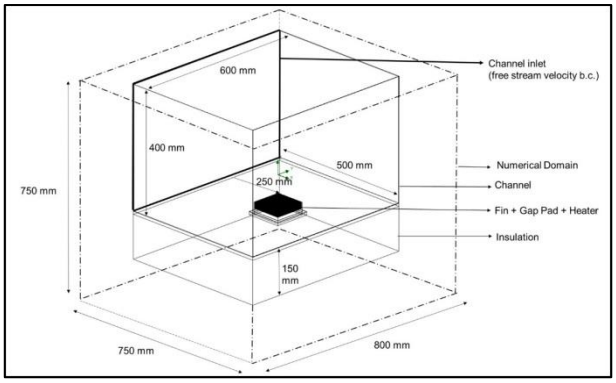

Figure 6. Numerical domain

Numerical analyses are conducted with Mentor Graphics' FLoEFD (2015a), which is a finite volume method based software. Second order upwind and central difference schemes are used for discretization of convective and diffusive terms, respectively. Analyses performed are based on Favre-Averaged Navier-Stokes (FANS) Equations presented in the technical reference of Mentor Graphics' FLoEFD (2015a) and MIT (2018). The governing equations are expressed as:

$$\frac{\partial \rho}{\partial t} + \frac{\partial (\rho u_i)}{\partial x_i} = 0 \tag{3}$$

$$\frac{\partial}{\partial t}(\rho u_i) + \frac{\partial}{\partial x_j}(\rho u_i u_j) = -\frac{\partial \rho}{\partial x_i} + \frac{\partial t_{ij}}{\partial x_j} \tag{4}$$

$$\frac{\partial}{\partial t}\left[\rho(e+\frac{1}{2}u_i u_i)\right] + \frac{\partial}{\partial x_j}\left[\rho u_j (h+\frac{1}{2}u_i u_i)\right] = \frac{\partial}{\partial x_j}\left(u_j t_{ij}\right) - \frac{\partial q_j}{\partial x_j} \tag{5}$$

Semi-Implicit Method for Pressure-Linked Equations (SIMPLE) is used for solving the linear algebraic systems obtained. SIMPLE algorithm is an iterative method including the setting of boundary conditions, computing velocity and pressure gradients, determining velocity and pressure fields, and then corrected mass fluxes, etc. as solution steps.

Steady state analyses with ambient temperature and pressure values set to 25℃ and 1 atm, are performed. Free-stream velocities are 3, 5 and 7 m/s at the inlet of the channel. The pressure for the outlet is defined as 1 atm. 150 W is applied as a heat source boundary condition. Numerical studies of Dong et al. (2010) and Yuan et al. (2012) that showed good agreement with the results of the turbulence model with the experimental ones are considered as the validation case for the selected k-ε turbulence model in this study. Mentor Graphics' FloEFD (2015b) uses Cartesian rectangular solid, fluid and partial cells. Denser mesh is used near the fin region as shown in Figure 7. Adaptive meshing technique is used for the solution.

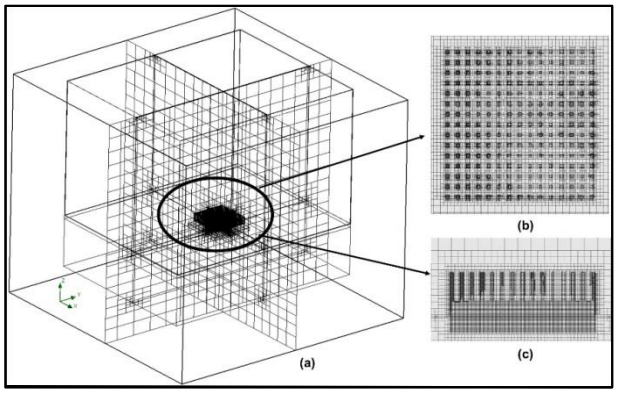

Figure 7. View of the mesh (a) for numerical domain, (b) from top of fin, (c) from side of fin

The accuracy of the numerical analysis is controlled by updating the convergence criteria for maximum temperature on the upper surface of the base plate. When the dispersion between the last iterations is below the convergence criteria, mesh refinement is applied and the procedure is repeated. In the present study, the minimum convergence criterion for the maximum temperature value difference between the successive iterations is selected to be 0.4℃.

RESULTS AND DISCUSSION

Experimental and Numerical Results

The visualization of the variation of maximum temperature on the surface of different geometry fins attached to heat sinks is performed. To achieve this, 63 different experiments and analyses considering 21 different geometries, 3 velocity values (3 m/s, 5 m/s and 7 m/s), heat input value of 150 W, and 25℃ ambient temperature are carried out at steady state conditions. S_L/L values resulting in minimum T_{max} at the upper face of surface plate are plotted. T_{max} values of square and cylindrical fins with S_L/L = 0.0208 and plate fins are compared and plotted in Figures 8–10 for 3 m/s velocity, respectively to illustrate agreement of numerical and experimental results.

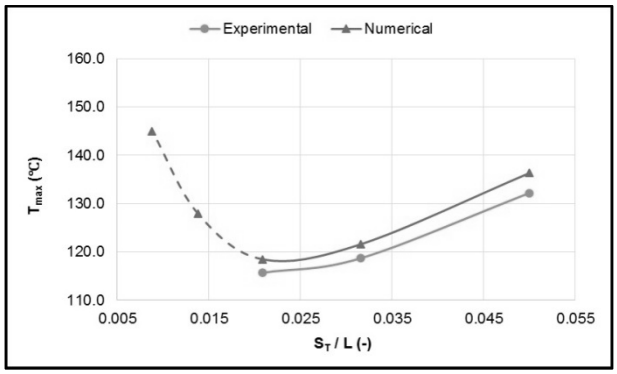

Figure 8. Square fins (S_L/L = 0.0208)

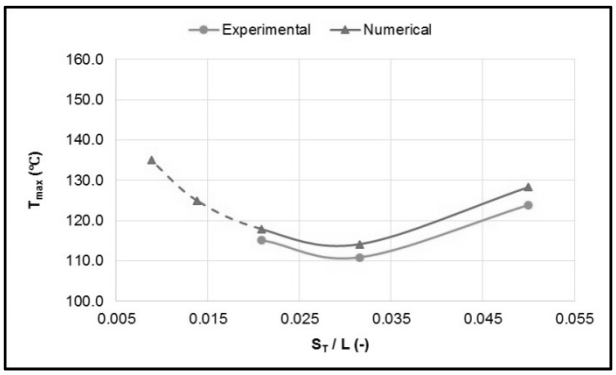

Figure 9. Cylindrical fins (S_L/L = 0.0208)

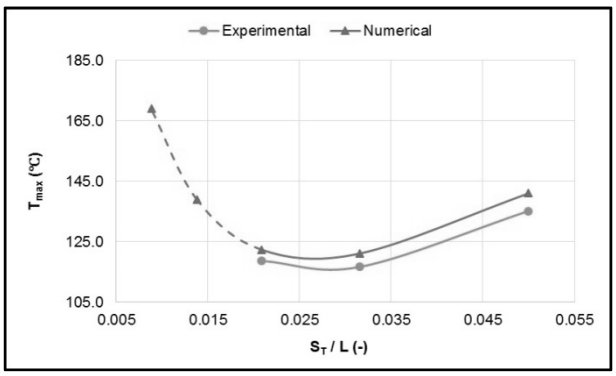

Figure 10. Plate fins

While keeping the other geometrical parameters constant, after the value of 0.0500, decreasing non-dimensional spanwise spacing value further increases heat transfer area hence enhances the heat transfer performance. But further reductions in non-dimensional spanwise spacing amplifies the pressure drop and offsets the positive effect of increasing heat transfer area on thermal performance.

Distribution of T_{max} values for the square (S_L/L = 0.0208, S_T/L = 0.0208), cylindrical (S_L/L = 0.0208, S_T/L = 0.0316) and plate (S_T/L = 0.0208) fins at 7 m/s free-stream velocity are illustrated in Figures 11-13, respectively.

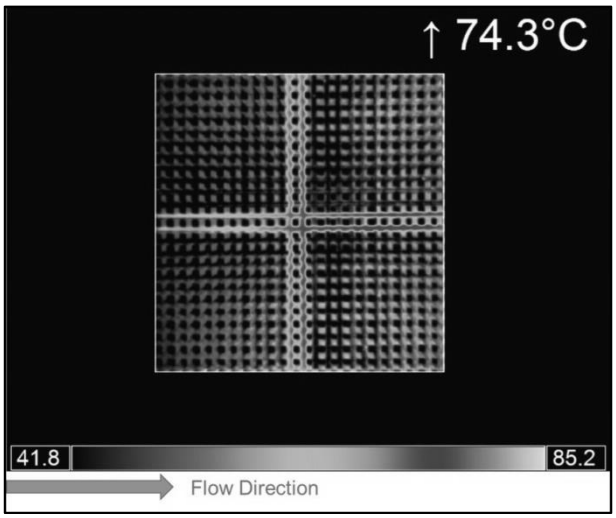

Figure 11. T_{max} for the square fin (S_L/L = 0.0208, S_T/L = 0.0208), U = 7 m/s

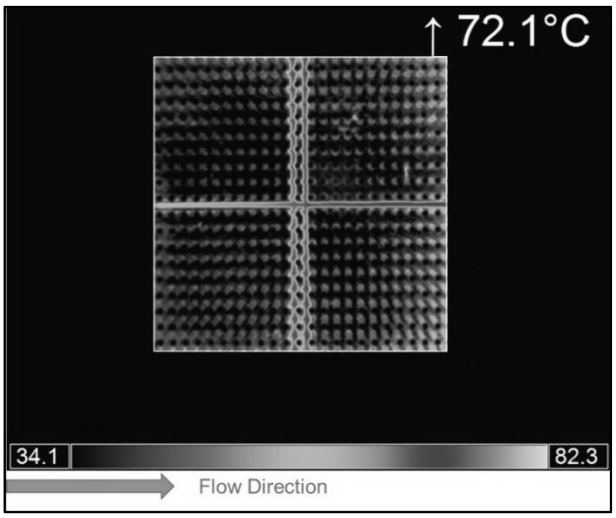

Figure 12. T_{max} for the cylindrical fin (S_L/L = 0.0208, S_T/L = 0.0316), U = 7 m/s

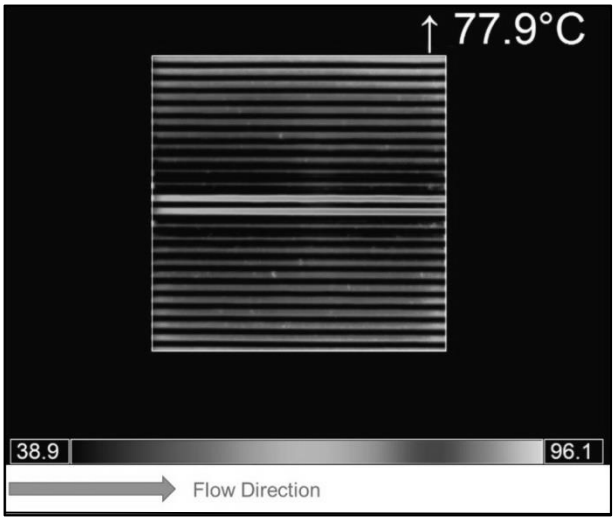

Figure 13. T_{max} for the plate fin (S_T/L = 0.0208), U = 7 m/s

As the tip of the fins is not shrouded, bypass occurs from the top of the fin in the streamwise direction. So, the mass flow rate of air enabling heat transfer decreases in the streamwise direction and temperature gradient occurs in this direction. Similarly, the maximum temperature is determined at the back side of the base plate in the numerical analysis. In contrast, there is more uniform temperature distribution in spanwise direction due to the symmetry.

Experimental Data and Uncertainty Analysis

Heat transfer correlations are obtained for determination of heat transfer from air cooled heat sinks without performing any analysis for well-defined ranges of the parameters. Convection heat transfer rate is calculated as follows:

$$Q_{input} = Q_{conv} + Q_{rad} + Q_{ins} \quad (6)$$

where Q_{input} denotes heat rate generated at the heater, Q_{conv} is the convection heat transfer rate through the

finned surface, and Q_{rad} is the radiation heat transfer rate from the fin. Q_{ins} is the heat transfer rate through the insulation layer and is calculated using Equation (7).

$$Q_{ins} = k_{ins} A_{ins} \frac{\Delta T}{L_{ins}} \tag{7}$$

Radiation heat transfer rate is calculated by assuming that the fin is almost completely surrounded by tunnel walls and the view factor between the fin and walls are taken as 1. The fin is assumed as a solid quadrangular, because the temperature gradient between neighboring fins is small as shown in Figure 14.

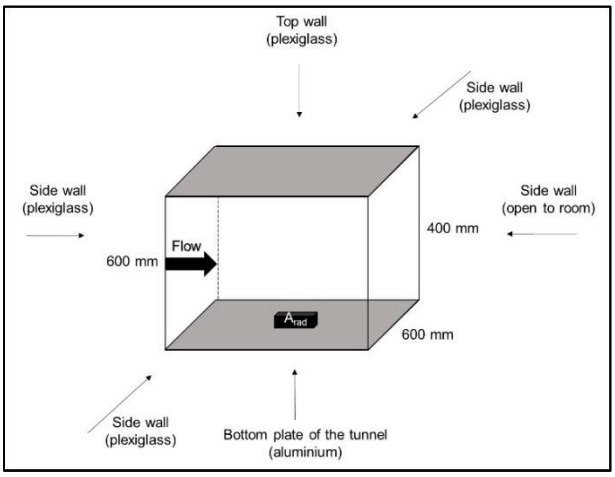

Figure 14. Enclosure representation for radiation calculation

Radiation calculations are performed based on temperatures of the surrounding channel walls (assumed to be equal to air inlet temperature) and the average base plate temperatures as given in Equation (8).

$$Q_{rad} = \frac{\sigma\left(T_{base\_ave}^4 - T_{surr}^4\right)}{\frac{1-\varepsilon_{fin}}{\varepsilon_{fin} A_{rad}} + \frac{1}{A_{rad} F_{(f)(surr)}} + \frac{1-\varepsilon_{surr}}{\varepsilon_{surr} A_{surr}}} \tag{8}$$

In Equation (8), ε_{fin} and ε_{surr} are emissivity values of unoxidized aluminum (0.2) presented in the datasheet of Optris' Pi 640 (2018) and plexiglass (0.86) presented in the Electronic Temperature Instruments (2018), respectively. Variables A_{rad}, A_{surr} and $F_{(f)(surr)}$ are radiation heat transfer area of finned sink (0.022 m^2), surrounding area of plexiglass walls as presented in Figure 14 (1.32 m^2) and view factor which is assumed to be unity, respectively. In Equation (8), base average temperature is calculated using Equations (9) and (10).

$$T_{base\_ave} = \frac{T_1 + T_2 + T_3 + T_4}{4} \tag{9}$$

(square and cylindrical fins) (see Figure 4)

$$T_{base\_ave} = \frac{T_1 + T_2}{2} \tag{10}$$

(plate fins) (see Figure 4)

Obtaining Q_{conv} using Equation (6), the average heat transfer coefficient value (h_{avg}) is calculated as provided by Bergman et al. (2011) as following:

$$Q_{conv} = h_{avg} A_T \eta_o \Delta T_{lm} \tag{11}$$

$$\Delta T_{lm} = \frac{\left(T_2 - T_{air\_o}\right) - \left(T_1 - T_{air\_i}\right)}{\ln\left(\frac{T_2 - T_{air\_o}}{T_1 - T_{air\_i}}\right)} \tag{12}$$

In Equation (11), A_T denotes total heat transfer area of the finned body, and η_o is the overall surface efficiency determined by standard fin analyses defined in Bergman et al. (2011). Variables T_1, T_2, T_{air_o} defined in Equation (12) are for determination of the logarithmic mean temperature difference between fin base plate and air temperature values at the back and front of the base plate, and average air temperature at the outlet, respectively.

After determination of h_{avg} using Equation (11) by false position method as presented in the study of Chapra and Canale (2015), Nusselt number is calculated such that:

$$Nu = \frac{h_{avg} D_h}{k_{air}} \tag{13}$$

Characteristic length (D_h) definition for Reynolds number calculation is valid for Nusselt number definition, too. Least square linear regression can be used for determination of heat transfer correlation as stated in Chapra and Canale (2015) and Ayli et al. (2016). The general form of the correlation can be represented as:

$$Nu_{corr} = aRe^b \left(\frac{S_T}{L}\right)^c \left(\frac{S_L}{L}\right)^e \tag{14}$$

$$\log\left(Nu_{corr}\right) = \log\left(a\right) + b\log\left(Re\right) + c\log\left(\frac{S_T}{L}\right) + e\log\left(\frac{S_L}{L}\right) \tag{15}$$

Error calculations are performed for clarifying the results presented in Figures 15–17. Heat transfer correlations based on Equations 16–20 derived from the study of Chapra and Canale (2015) are used. The results related to the corresponding Equations are presented in Table 3.

$$\overline{Nu_{exp}} = \frac{\sum Nu_{exp}}{n} \tag{16}$$

$$S_t = \sum\left(Nu_{exp} - \overline{Nu_{exp}}\right)^2 \;\&\; S_y = \sqrt{\frac{S_t}{n-1}} \tag{17}$$

Table 3. Error analysis of heat transfer correlation for all fins

	$\overline{Nu_{exp}}$	ΣS_t	ΣS_r	S_y	$S_{y/x}$	$S_{y/x} < S_y$	C.V.%	r^2 %	r
Square	2.75	15.79	0.61	0.78	0.16	√	28.29	96.13	0.98
Cylindrical	3.71	33.81	1.15	1.14	0.22	√	30.73	96.59	0.98
Plate	2.03	2.03	0.17	0.50	0.17	√	24.83	91.53	0.96

$$C.V. = \frac{S_y}{\overline{Nu_{exp}}} 100\% \quad (18)$$

$$S_r = \sum \left(Nu_{exp} - Nu_{corr} \right)^2 \;\&\; S_{y/x} = \sqrt{\frac{S_r}{n-y-1}} \quad (19)$$

In Equation (19), predictor variable (y) is 3 for square and cylindrical fins and 2 for plate fins. If, $S_{y/x} < S_y$, linear regression model has merit. So, coefficient of determination (r^2) and correlation coefficient (r) can be determined as:

$$r^2 = \frac{S_t - S_r}{S_t} 100\% \;\&\; r = \sqrt{\frac{S_t - S_r}{S_t}} \quad (20)$$

Correlations for square and cylindrical fins are plotted in Figures 15 and 16, respectively. In the range of 509.2≤Re≤1752,2 and 0.0208 ≤ S_T/L & S_L/L ≤0.0500 the correlation obtained for square fins can be used. The correlation derived for cylindrical fins is valid in the range of 485.1 ≤ Re≤1682.7 and 0.0208 ≤ S_T/L & S_L/L ≤0.0500.

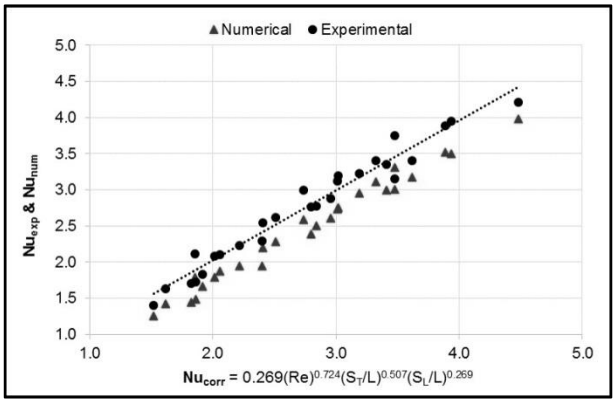

Figure 15. Heat transfer correlation for square fins

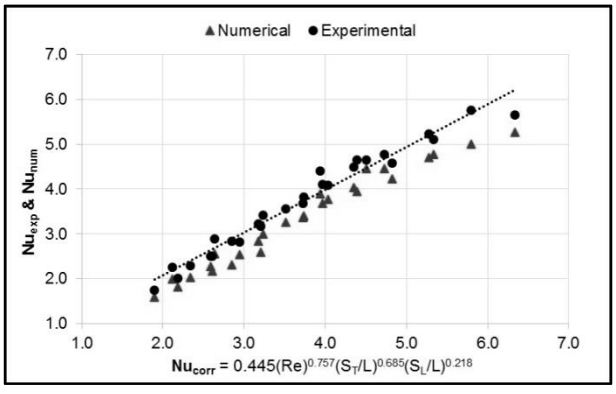

Figure 16. Heat transfer correlation for cylindrical fins

In a similar study conducted by Jubran et. al (1993) for cylindrical fins, the following correlation is determined:

$$Nu_{corr} = 0.580 (\mathrm{Re})^{0.510} \left(\frac{S_T}{L} \right)^{0.180} \left(\frac{S_L}{L} \right)^{0.210}$$
$$5x10^3 \le Re \le 5x10^4 \quad (21)$$

Correlation for cylindrical fins in the current work is:

$$Nu_{corr} = 0.445 (\mathrm{Re})^{0.757} \left(\frac{S_T}{L} \right)^{0.685} \left(\frac{S_L}{L} \right)^{0.218} \quad (22)$$

In Jubran's study (1993), Reynolds number range is greater than that of the present study, so coefficients of the correlation in their study is larger than the present study. Fin array is unshrouded from tip in both studies, but fin array is shrouded from the sides perpendicular to the flow direction in Jubran's study unlike the present one. Therefore, correlation in the study of Jubran (1993) is less sensitive to changes in the number of fins in the spanwise direction. There is agreement between the coefficient of non-dimensional streamwise spacing.

Correlation for plate fins is presented in Figure 17. The validity range of the obtained correlation for plate fins is 502.6≤Re≤1619.3 and 0.0208≤ S_T/L & S_L/L ≤0.0500.

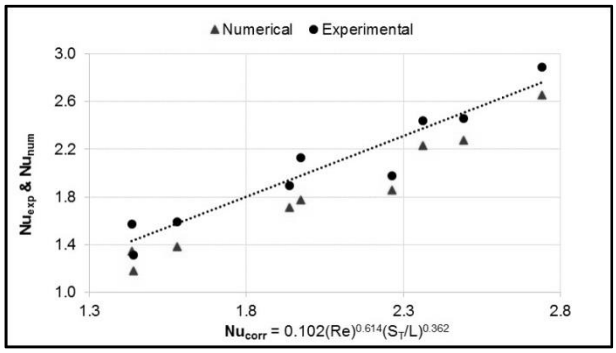

Figure 17. Heat transfer correlation for plate fins

This study differs from others in literature because, general correlations are derived at the same time for fins with different profiles and their heat transfer performance are compared in terms of correlation coefficients.

Heat transfer augmentation of cylindrical fins become more dominant than square and plate ones with increasing velocity. It can be observed from power coefficient of Reynolds number "b" in correlation equations, too. It has values of 0.724, 0.757 and 0.614 for

square, cylindrical and plate fins, respectively. Superiority of cylindrical fins can be explained with a phenomenon called as Coanda effect mentioned in the study of Yang et al. (2007). Flow field separation from the curved bodies occurs late. So, cylindrical fins benefit maximum from flow field, although, total heat transfer area of cylindrical fins are lower than square and plate ones. Coefficients of heat transfer correlations can be used to comment on heat transfer performance of fins. Correlation coefficient "a" of cylindrical fins is found as 0.445, while it has a value of 0.269 and 0.102 for square fins and plate fins, respectively.

Uncertainty analysis is performed based on the study of Moffat (1988). First order analysis is conducted by only considering variable (measurement) errors. Uncertainty of Q_{conv} can be calculated based on equation:

$$\delta Q_{conv} = \sqrt{\left(\delta Q_{input}\right)^2 + \left(-\delta Q_{rad}\right)^2 + \left(-\delta Q_{ins}\right)^2} \quad (23)$$

Uncertainty of Q_{input}, Q_{rad} and Q_{ins} can be calculated as follows:

$$\delta Q_{input} = \sqrt{\left(I\delta V\right)^2 + \left(V\delta I\right)^2} \quad (24)$$

$$\delta Q_{rad} = \sqrt{\left(\sigma\varepsilon A_{rad} F_{(f)(surr)}\right)^2 \begin{pmatrix} \left(T_{base\_ave}\right)^6 (\delta T_1^2 + \\ \delta T_2^{\,2} + \delta T_3^{\,2} + \delta T_4^{\,2}) + \\ \left(-4\left(T_{surr}\right)^3 \delta T_{surr}\right)^2 \end{pmatrix}} \quad (25)$$

$$\delta Q_{ins} = \sqrt{\frac{A_{ins}^{\,2}}{L_{ins}^{\,2}} \begin{pmatrix} \left(\left(T_5 - T_6\right)\delta k_{ins}\right)^2 + \\ \left(k_{ins}\delta T_5\right)^2 + \left(-k_{ins}\delta T_6\right)^2 \end{pmatrix}} \quad (26)$$

Here, V and I denote voltage and current, respectively. T_5 and T_6 are the bottom temperatures of heater and insulation material. ΔT_{lm} term can be sent to the left-hand side of Equation (11) and uncertainty at the left-hand side of the equation can be found as:

$$\delta\left(\frac{Q_{conv}}{\Delta T_{lm}}\right) = \sqrt{\left(\frac{\delta Q_{conv}}{\Delta T_{lm}}\right)^2 + \left(\frac{-Q_{conv}}{\left(\Delta T_{lm}\right)^2}\delta\Delta T_{lm}\right)^2} \quad (27)$$

After adding deviations obtained from Equation (27), right-hand side of Equation (27) is solved again to find the uncertainty at average heat transfer coefficient (h_{avg}) with False position Method. Four numerical calculations are performed with the combinations of positive and negative values of δQ_{conv} and $\delta\Delta T_{lm}$, then absolute maximum deviation value among four results is accepted as δh_{avg}. Uncertainty at Nusselt number can be calculated using Equation (28).

$$\delta Nu = \sqrt{D_h^{\,2}\left(\left(\frac{\delta h_{avg}}{k_{air}}\right)^2 + \left(\frac{-h_{avg}}{k_{air}^{\,2}}\delta k_{air}\right)^2\right)} \quad (28)$$

Maximum uncertainty values of average heat transfer coefficient and Nusselt number for each of the square, cylindrical and plate fins are presented in Table 4.

Table 4. Maximum uncertainty values for square, cylindrical and plate fins

Geometry	% h_{avg}	% Nu
Square	3.202	3.207
Cylindrical	3.909	3.914
Plate	3.187	3.194

CONCLUSION

Minimum T_{max} occurring for square, cylindrical and plate fins are observed as 115.7℃, 110.9℃ and 116.7℃, respectively. The most important finding of this study is the observation of superior heat transfer performance of cylindrical fins with respect to other geometries at the same velocity and Reynolds number. This fact can also be observed when the correlation coefficients are examined. Coanda effect, as illustrated in Figure 18, is the physical phenomenon behind the mentioned performance of cylindrical fins.

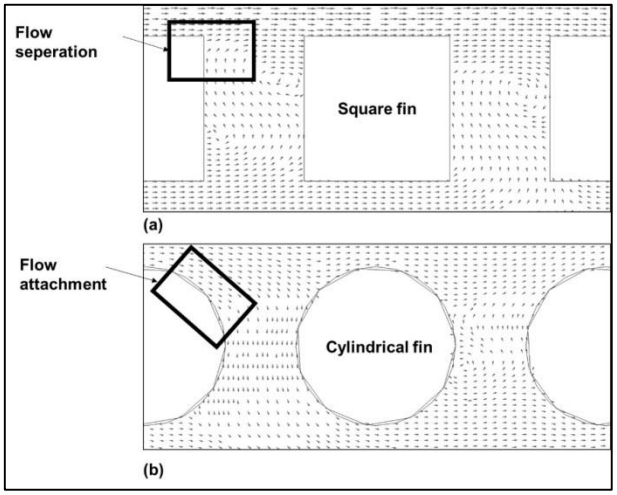

Figure 18. Hydrodynamic behavior of flow near (a) square fin (b) cylindrical fin

Heat transfer rate through insulation layer can be considered as one of the reasons for discrepancy between the numerical and experimental results, although insulation measures are reflected in the numerical model. The insulation material is placed in layers in the experiment, but it is modeled as bulk in numerical studies. Therefore, contact problems may occur between layers of insulation material and heat can be transferred outside in the lateral direction to the insulation. Moreover, edges of the fins are placed 10 mm on each side away from the bottom aluminum plate of the tunnel to avoid conduction between the fin and tunnel bottom plate. The gap between the tunnel and fin is filled with

insulation material. It is very difficult to cut and place it in exact dimensions as it is very soft material, so insulation material is placed in particles to fill this gap and unaccounted losses may occur from this region, unlike the numerical model. Furthermore, there are rigid electrical cables, which are not considered in the numerical model, below the heater. Difficulties to insulate these cables could result in the gap around them and undesired losses may happen. Heater, gap pad and fin are perfectly mounted to each other in the numerical model, but contact problems may occur between these components in the experimental setup and conduction heat transfer rates to the fin may be reduced.

As an extension of this work, flow visualization techniques can be used in experiments to further understand the flow field around fin. Moreover, streamwise and spanwise spacing values around the optimum point can be discretized more intensely to define more accurate design points in both directions. Furthermore, staggered alignment of fins can be studied and comparison of heat transfer performance can be done.

ACKNOWLEDGMENT

This work is supported by Aselsan Inc., Turkey.

REFERENCES

A-Damook, A., Summers, J. L., Kapur, N. and Thompson, H., 2016, Effect of Temperature-Dependent Air Properties on the Accuracy of Numerical Simulations of Thermal Airflows over Pinned Heat Sinks, *Int. Communications in Heat and Mass Transfer*, 78, 163-167.

Ayli, E., Bayer, O. and S. Aradag, 2016, Experimental Investigation and CFD Analysis of Rectangular Profile Fins in a Square Channel for Forced Convection Regimes, *Int. J. Therm. Sci*., 109, 279-290.

Babus'Haq, R. F., Akintunde, K. and Probert, S. D., 1995, Thermal Performance of a Pin-Fin Assembly, *Int. J. Heat Fluid Flow*. 16, 50-55.

Culham, J. R. and Muzychka, Y. S., 2001, Optimization of Plate Fin Heat Sinks Using Entropy Generation Minimization, *IEEE Trans. Components Packag. Technol.*, 24, 159-165.

Chapra, S. C. and Canale, R. P., 2015, *Numerical Methods for Engineers*, (7th Ed.) McGraw-Hill, New York.

Chu, P., He, Y. L., Xu, R. J. and Han, H., 2011, Experimental and Numerical Study on Natural Air Cooling of a Remote Radio Unit, *Journal of Enhanced Heat Transfer*, 18, 345-359.

Deshmukh, P.A., 2013, Comparison of Thermal Performance of Circular and Elliptical Pin Fin Heat Sinks in Assisting Mixed Convection, *IEEE*, 50, 178-184.

Diani, A., Mancin, S., Zilio, C. and Rossetto, L., 2013, An Assessment on Air Forced Convection on Extended Surfaces: Experimental Results and Numerical Modeling, *Int. J. Therm. Sci.*, 67, 120-134.

Dong, J., Chen, J., Zhang, W. and J. Hu, 2010, Experimental and Numerical Investigation of Thermal-Hydraulic Performance in Wavy Fin-and-Flat Tube Heat Exchangers, *Appl. Therm. Eng.*, 30, 1377-1386.

Electronic Temperature Instruments, *Emissivity Table*, accessed February 12, 2018 from https://thermometer.co.uk/img/documents/emissivity_table.pdf.

European Association of National Metrology Institutes, *Calibration Guidelines*, accessed December 29, 2018, from https://www.euramet.org/publications-media-centre/ calibration-guidelines/.

Incropera, F. P. and Dewitt, D. P., Bergman, T. L., Lavine, A. S., 2013, *Introduction to Heat Transfer* (7th Ed.), John Wiley & Sons Inc, Singapore.

Jonsson, H. and Moshfegh, B., 2001, Modeling of the Thermal and Hydraulic Performance of Plate Fin, Strip Fin, and Pin Fin Heat Sinks-Influence of Flow Bypass, *IEEE Trans. Components Packag. Technol.*, 24, 142-149.

Jubran, B. A., Hamdan M. A. and Abdullah, R. M., 1993, Enhanced Heat Transfer, Missing Pin, and Optimization for Cylindrical Pin Fin Arrays, *Journal of Heat Transfer*, 115, 576-583.

Kanargi, B., Lee, P. S. and Yap, C., 2018, A Numerical and Experimental Investigation of Heat Transfer and Fluid Flow Characteristics of an Air-Cooled Oblique-Finned Heat Sink, *Int. J. of Heat and Mass Transfer*, 116, 393-416.

Khan, W. A., 2004, *Modeling of Fluid Flow and Heat Transfer for Optimization of Pin-Fin Heat Sinks*, PhD Thesis, University of Waterloo.

Kwak, D-B., Noh, J-H., Lee, K-S. And Yook, S-J., 2017, Cooling Performance of a Radial Heat Sink with Triangular Fins on a Circular Base at Various Installation Angles, *Int. J. of Thermal Science*, 120, 377-385.

Mentor Graphics, *FloEFD Technical Reference V14*, Oregon: Mentor Graphics Corporation, pp. 238, 2015a.
Mentor Graphics, *Solving Engineering Problems*, Oregon: Mentor Graphics Corporation, p. 98, 2015b.

MIT, *Turbulence Modeling*, accessed February 12, 2018 from http://web.mit.edu/cuongng/www/Site/Publication_files/TurbulenceModeling_04NOV05.pdf.

Moffat, R. J., 1998, Describing the Uncertainties in Experimental Results, *Exp. Therm. Fluid Sci*., 1, 3-17.

Mohammadian, S.K. and Zang, Y., 2015, Thermal Management Optimization of an Air-Cooled Li-Ion Battery Module Using Pin-Fin Heat Sinks for Hybrid Electric Vehicles, *Journal of Power Sources*, 273, 431-439.

OPTRIS, *Datasheet Pi 640*, accessed February 12, 2018 from http://www.optris.com.tr/infrared-cameras.

Sahiti, N., Lemouedda, A., Stojkovic, D., Durst, F. and Franz, E., 2006, Performance Comparison of Pin Fin in-Duct Flow Arrays with Various Pin Cross-Sections, *Appl. Therm. Eng.*, 26, 1176-1192.

Samarth, A. B. and Sawankar, K. S., 2014, Thermal Performance of Perforated Pin-Fin Arrays in Staggered Arrangement, *International Journal of Scientific & Engineering Research*, 5, 777-783.

Sandhu, H., Gangacharyulu, D., and Singh, M. K., 2014, Experimental Investigations on the Cooling Performance of Microchannels Using Alumina Nanofluids with Different Base Fluids", *Journal of Enhanced Heat Transfer*, 25, 283-291.

Tahat, M., Kodah, Z. H., Jarrah, B. A. and Probert, S. D., 2000, Heat Transfers from Pin-Fin Arrays Experiencing Forced Convection, *Applied Energy*, 67, 419-442.

Yang, K. S., Chu, W. H., Chen, I. Y. and Wang, C. C., 2007, A Comparative Study of the Airside Performance of Heat Sinks Having Pin Fin Configurations, *Int. J. Heat Mass Transf.*, 50, 4661-4667.

Yang, Y. T., Peng, H. S. and Hsu, H. T., 2013, Numerical Optimization of Pin-Fin Heat Sink with Forced Cooling, *International Journal of Electrical, Computer, Energetic, Electronic and Communication Engineering*, 7, 884-891.

Yuan, W., Zhao, J., Tso, C. P., Wu, T., Liu W. and T. Ming, 2012, Numerical Simulation of the Thermal Hydraulic Performance of a Plate Pin Fin Heat Sink, *Appl. Therm. Eng.*, 48, 81-88.

Zukauskas, A., 1972, *Heat Transfer From Tubes in Crossflow*, Vilnius: Academy of Sciences of the Lithuanian SSR, 93-160.

Aykut Barış İNCİ He received his BS degree from Mechanical Engineering Department, Middle East Technical University, in 2012 and completed his M.Sc. in 2018 at the same university. He has been working as mechanical design engineer for Aselsan since 2012.

Özgür BAYER Dr. Bayer graduated from Mechanical Engineering Department, Middle East Technical University, in 2000. He got his M.Sc. and Ph.D. degrees at the same university in 2002 and 2009, respectively. His research interests are thermodynamics, experimental and numerical heat transfer, refrigeration, radiative cooling and HVAC&R Systems.